Impact of CCD camera SNR on polarimetric accuracy

Zhenyue Chen,[1,2] Xia Wang,[1] Shaun Pacheco,[2] and Rongguang Liang[2,*]

[1]Key Laboratory of Photoelectronic Imaging Technology and System, School of Optoelectronics, Beijing Institute of Technology, Beijing 100081, China

[2]College of Optical Sciences, The University of Arizona, Tucson, Arizona 85721, USA

*Corresponding author: rliang@optics.arizona.edu

Received 20 August 2014; revised 10 October 2014; accepted 10 October 2014; posted 13 October 2014 (Doc. ID 221376); published 4 November 2014

A comprehensive charge-coupled device (CCD) camera noise model is employed to study the impact of CCD camera signal-to-noise ratio (SNR) on polarimetric accuracy. The study shows that the standard deviations of the measured degree of linear polarization (DoLP) and angle of linear polarization (AoLP) are mainly dependent on the camera SNR. With increase in the camera SNR, both the measurement errors and the standard deviations caused by the CCD camera noise decrease. When the DoLP of the incident light is smaller than 0.1, the camera SNR should be at least 75 to achieve a measurement error of less than 0.01. When the input DoLP is larger than 0.5, a SNR of 15 is sufficient to achieve the same measurement accuracy. An experiment is carried out to verify the simulation results. © 2014 Optical Society of America

OCIS codes: (120.4570) Optical design of instruments; (120.4640) Optical instruments; (040.1520) CCD, charge-coupled device; (120.5410) Polarimetry; (260.5430) Polarization.

http://dx.doi.org/10.1364/AO.53.007649

1. Introduction

Polarization imaging can highlight objects by acquiring both the intensity and the polarization information of a scene, while reducing the impact of the complex background; thus, it has great potential in target detection and identification [1–3]. Much research has been done on polarization imaging design [4–6], polarization property measurement [7,8], polarization image processing [9,10], etc. The polarization measurement accuracies of the degree of polarization, degree of depolarization, angle of polarization, retardance, and diattenuation are generally lower than those in intensity imaging systems. They are impacted by a number of factors, such as defects in wave plates and polarizers, light source characteristics, target properties, atmosphere transmission, and camera noises. Defects in wave plates include nonideal retardance, retardance axis variation, spatial nonuniformity, chromatic variation, and depolarization. Defects in polarizers include nonideal diattenuation, elliptical polarization, depolarization, and spatial nonuniformity. Errors caused by the camera include dark current, pixel offset, gain variations, etc. [11].

In order to achieve higher polarimetric accuracy, calibration and error analysis are necessary. Smith investigated the defects of polarization optical elements [12]. Masiero *et al.* presented the design and calibration method for the Dual-Beam Imaging Polarimeter [13]. Feng *et al.* presented a simple approach for estimating errors in the degree of linear polarization (DoLP) caused by radiometric measurement uncertainty [14]. However, there is a lack of comprehensive study on the impact of detector noise on polarimetric accuracy. Since detector noise will degrade the polarimetric accuracy, it is important to take this into consideration when performing precise polarization measurement or polarimetry system design or optimization.

In this paper, we investigate the impact of charge-coupled device (CCD) camera noise on polarimetric accuracy. The camera signal-to-noise ratio (SNR) is

1559-128X/14/327649-08$15.00/0

utilized to study the impact of camera noise on polarimetric accuracy at different luminous exposures. At different SNRs, we have analyzed the impacts of CCD camera noise on the DoLP and the angle of linear polarization (AoLP). Three linear analyzer orientations (0°, 60°, and 120°) are chosen to assure optimized measurements according to the condition number of the measurement matrix, and a detailed discussion is given in Section 3.

2. CCD Camera Noise Model

Several CCD camera noise models have been developed. Healy and Kondepudy modeled camera noise in measuring scene variation, including offset fixed-pattern noise (FPN), photon and dark-current shot noises, photoresponse nonuniformity (PRNU), and read-noise equivalent [15]. Boie and Cox analyzed CCD and vidicon camera noises, such as photon shot and electronic shot noise, dark-current, and readout noise [16]. Farrell *et al.* described a noise model that includes readout noise, dark-current, offset FPN, PRNU, and photon shot noise [17]. Irie and co-workers presented a comprehensive measurement of CCD digital-video camera noise based on the physical characteristics in the acquisition and sampling of photons through the image capture process [18,19]. The model incorporates all noise sources, including PRNU, photon shot noise (SN_{ph}), offset FPN, dark-current shot noise (SN_{dark}), readout noise (N_{read}), demosaicing noise (N_D), digital filtering noise (N_{filt}), as well as quantization noise (N_Q). In this model, the image, I_{cap}, is represented by

$$I_{\text{cap}} = (I + I \times \text{PRNU} + SN_{\text{ph}}(I) + \text{FPN} + SN_{\text{dark}} + N_{\text{read}}) \times N_D \times N_{\text{filt}} + N_Q(I_{\text{filt}}), \quad (1)$$

where I is an image without noise. Since this noise model is more comprehensive and can be calibrated with measured data, we use this model in our study.

3. Modeling and Simulation Fundamentals

A. Polarization Imaging System

Figure 1(a) shows a simple model of an optical system with CCDs. The flux collected by the CCD at wavelength λ is given by [20]

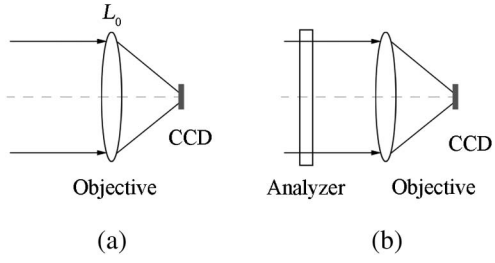

Fig. 1. Schematic diagrams of imaging systems: (a) intensity imaging and (b) polarization imaging.

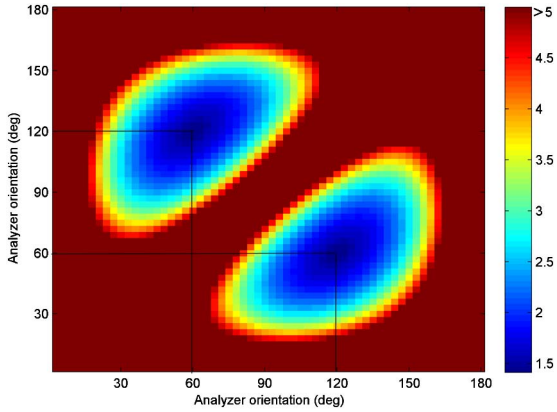

Fig. 2. Condition number map versus combinations of linear analyzer orientations. One of the three orientations is fixed as 0°. The horizontal and vertical axes represent the other two angles of orientation. The color bar shows the condition number. It can be seen that the combination of 0°, 60°, and 120° has the smallest condition number.

$$\Phi_0(\lambda) \cong \frac{\pi\tau_0(\lambda)}{4(f/\#)^2} L_{\text{scene}} lh, \quad (2)$$

where L_{scene} is the scene irradiance, $\tau_0(\lambda)$ is optical transmission at wavelength λ, l and h are, respectively, the width and the height of the CCD sensor, and $f/\#$ is the effective f-number of the lens. The simplest configuration of a polarization imaging system is to place an analyzer in front of the camera to select the detected polarization state, as shown in Fig. 1(b). The Stokes vector $S = [I, Q, U, V]^{\text{T}}$ is typically used to describe the polarization state of the light. In this study, we only study the measurement accuracies of the linear polarization properties. The normalized input Stokes vector is described by $S_{\text{in}} = [I_{\text{in}}, Q_{\text{in}}, U_{\text{in}}, 0]^{\text{T}}$. For the polarization measurement system shown in Fig. 1(b), the orientation of the linear analyzer, θ, is measured from the x axis. The Muller matrix of the linear analyzer with the transmission axis oriented at an angle θ can be described by $LP(\theta)$:

$$LP(\theta) = \frac{1}{2}\begin{bmatrix} 1 & \cos 2\theta & \sin 2\theta & 0 \\ \cos 2\theta & \cos^2 2\theta & \sin 2\theta \cos 2\theta & 0 \\ \sin 2\theta & \sin 2\theta \cos 2\theta & \sin^2 2\theta & 0 \\ 0 & 0 & 0 & 0 \end{bmatrix}. \quad (3)$$

Since the detector can only measure the flux, only the first row in the analyzer's Muller matrix is used to

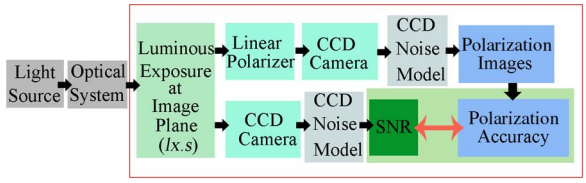

Fig. 3. Simulation block diagram.

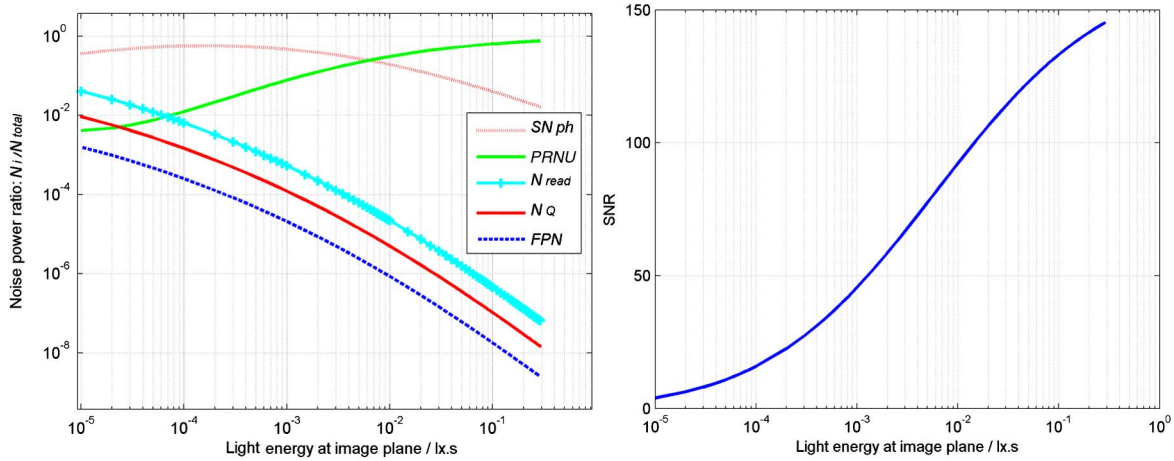

(a) (b)

Fig. 4. Noise power ratio and SNR versus input luminous exposure. (a) A plot of the noise power ratio of the primary noises in the model and (b) a plot of the SNR.

calculate the flux transmitted. The flux detected can be described by

$$P_\theta = \frac{1}{2}(I_{\text{in}} + Q_{\text{in}} \cos 2\theta + U_{\text{in}} \sin 2\theta)\Phi_0. \quad (4)$$

A linear polarization measurement is a set of measurements acquired with a set of linear analyzer orientations. Let the total number of orientations be N; then the polarimetric measurement matrix W can be described by [11]

$$W = \frac{1}{2}\begin{bmatrix} 1 & \cos 2\theta_1 & \sin 2\theta_1 & 0 \\ 1 & \cos 2\theta_2 & \sin 2\theta_2 & 0 \\ \vdots & \vdots & \vdots & \vdots \\ 1 & \cos 2\theta_N & \sin 2\theta_N & 0 \end{bmatrix}. \quad (5)$$

The N measured fluxes are arranged in a measurement vector $P = \{P_0, \quad P_1, \quad \cdots \quad P_N\}^{\text{T}}$. P is related to S_{in} by the polarimetric measurement equation

$$P = W \cdot S_{\text{in}} \cdot \Phi_0. \quad (6)$$

To retrieve the input polarization state S_{in}, at least three measurements are needed. According to polarization measurement theories [6,21,22], a polarimeter has the lowest noise sensitivity when the condition number of the measurement matrix, W, is the smallest [23]. The condition numbers of different combinations of analyzer orientations, for instance, three orientations and four orientations, are investigated. According to the condition number calculation, both combinations have the smallest condition number, 1.4142. For the four-orientation combination, the smallest condition number corresponds to an angle increment of 45°, while for the three-orientation combination, the smallest condition number corresponds to an angle increment of 60° as shown in Fig. 2. The combination of 0°, 60°, and 120° is chosen to assure that the system has the best noise immunity.

In the simulation, Img_0, Img_{60}, and Img_{120} are employed to represent the three acquired linear polarization images. Now Eq. (5) can be revised as

$$\begin{bmatrix} \text{Img}_0 \\ \text{Img}_{60} \\ \text{Img}_{120} \end{bmatrix} = \frac{1}{2}\begin{bmatrix} 1 & 1 & 0 & 0 \\ 1 & -\frac{1}{2} & \frac{\sqrt{3}}{2} & 0 \\ 1 & -\frac{1}{2} & -\frac{\sqrt{3}}{2} & 0 \end{bmatrix}\begin{bmatrix} I_{\text{in}} \\ Q_{\text{in}} \\ U_{\text{in}} \\ 0 \end{bmatrix}. \quad (7)$$

So the input Stokes vector can be retrieved as

$$\begin{aligned} \hat{I}_{\text{in}} &= 2/3(\text{Img}_0 + \text{Img}_{60} + \text{Img}_{120}) \\ \hat{Q}_{\text{in}} &= 4/3(\text{Img}_0 - 1/2\text{Img}_{60} - 1/2\text{Img}_{120}) \\ \hat{U}_{\text{in}} &= 2/\sqrt{3}(\text{Img}_{60} - \text{Img}_{120}). \end{aligned} \quad (8)$$

The DoLP and AoLP can be calculated, respectively, as

$$\begin{aligned} \text{DoLP} &= \frac{\sqrt{\hat{Q}_{\text{in}}^2 + \hat{U}_{\text{in}}^2}}{\hat{I}_{\text{in}}} \\ &= \frac{\sqrt{(2I_{\text{out0}} - I_{\text{out60}} - I_{\text{out120}})^2 + 3(I_{\text{out60}} - I_{\text{out120}})^2}}{I_{\text{out0}} + I_{\text{out60}} + I_{\text{out120}}}, \end{aligned} \quad (9)$$

Table 1. Camera Parameters

Parameter Name	Value
Charge conversion factor K_f (uV/e–)	6
Quantum efficiency η (at 0.6 μm)	0.8
Sensitivity R (V/(lx · s))	9
Pixel number $H \times V$	1280 × 1024
Integration time τ_d (ms)	1
Saturation luminous exposure (lx · s)	0.30

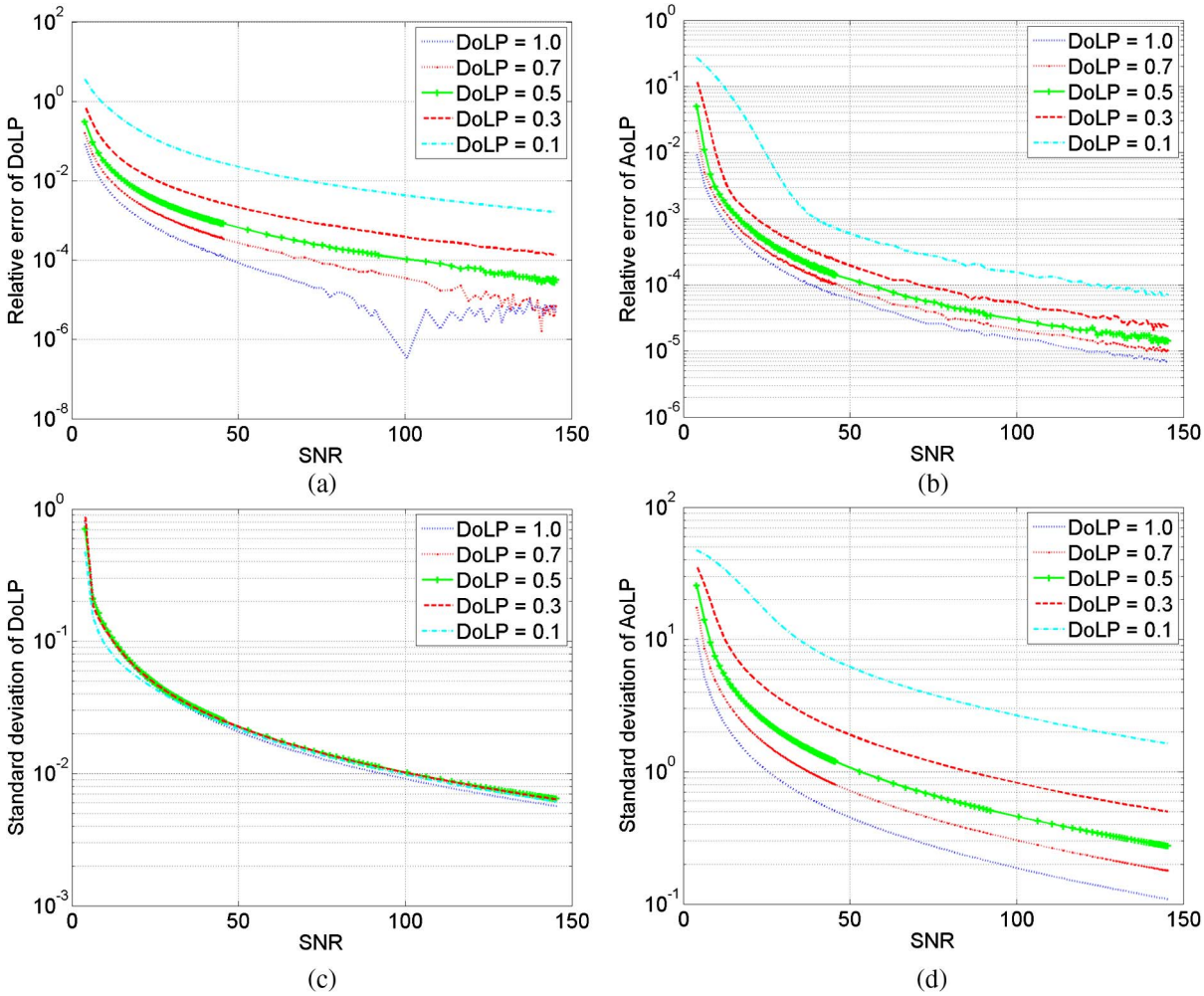

Fig. 5. Measurement error versus DoLP and SNR. (a) Relative error of the acquired DoLP. (b) Relative error of the acquired AoLP. (c) Standard deviation of the acquired DoLP versus the SNR. (d) Standard deviation of the acquired AoLP versus the SNR.

$$\mathrm{AoLP} = \frac{1}{2}\arctan\left(\frac{\hat{U}_{\mathrm{in}}}{\hat{Q}_{\mathrm{in}}}\right) = \frac{1}{2}\arctan\left(\frac{\sqrt{3}(I_{\mathrm{out60}} - I_{\mathrm{out120}})}{2I_{\mathrm{out0}} - I_{\mathrm{out60}} - I_{\mathrm{out120}}}\right). \quad (10)$$

B. Simulation Model

The image quality of the CCD camera is determined by a number of factors, such as the input light intensity, optical transmission, and camera sensitivity. To focus the study on CCD camera noise, luminous exposure at the image plane is used as the initial input. Luminous exposure is expressed in lux seconds ($\mathrm{lx}\cdot\mathrm{s}$), the product of lux (lx) and seconds (s), as determined by shutter speed, lens aperture, and scene luminance. Luminous exposure was varied in the simulation to generate SNR variations in the camera images. The definition of SNR employed in this paper is the ratio of the average signal value, μ_{sig}, to the standard deviation of the signal, σ_{sig}, as shown in Eq. (11) [24]:

$$\mathrm{SNR} = \frac{\mu_{\mathrm{sig}}}{\sigma_{\mathrm{sig}}}. \quad (11)$$

Taking the CCD camera noise model into consideration, three linear polarization images are generated

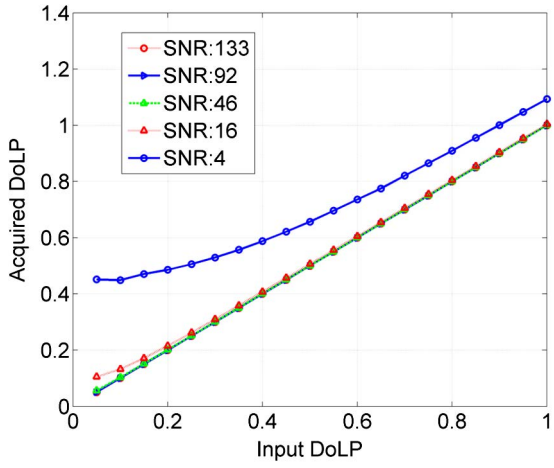

Fig. 6. Acquired DoLP versus input DoLP and SNR.

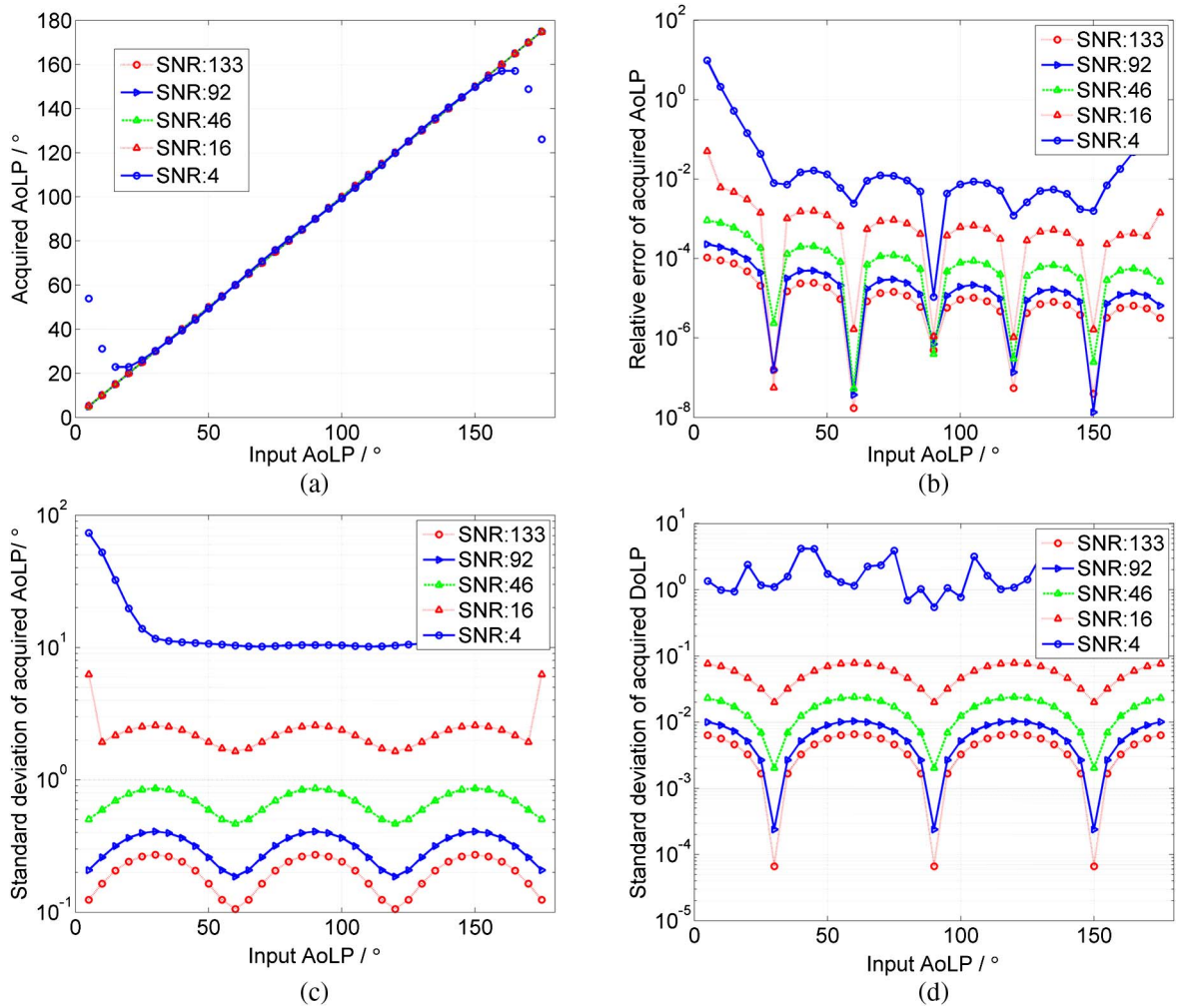

Fig. 7. Measurement error with different input AoLPs. (a) Acquired AoLP. (b) Relative error of the acquired AoLP versus the input AoLP and the SNR. (c) Standard deviation of the acquired AoLP versus the input AoLP and the SNR. (d) Standard deviation of the acquired DoLP versus the input AoLP and the SNR.

according to the polarization imaging principle described in Section 3.A. We use "input DoLP" and "input AoLP" to change the polarization state of the incident light. "Acquired DoLP" and "acquired AoLP" are employed to represent the polarization state retrieved. We use relative error and standard deviation to evaluate the errors between the retrieved DoLP, AoLP, and their input values. The term polarimetric accuracy is defined as the degree to which the polarization parameters retrieved conform to their true values. Finally, the relationship between SNR and polarimetric accuracy is established. A simulation block diagram is shown in Fig. 3.

4. Simulation Results and Analysis

The camera parameters used in this study are listed in Table 1. The luminous exposure range is chosen to be $10^{-5} - 0.3$ lx · s in order to assure that the camera SNR is not dominated by noise. The corresponding noise power ratio plot of each camera noise is shown in Fig. 4(a) and the camera SNR is shown in Fig. 4(b). In Fig. 4(a), it can be seen that when the luminous exposure is very weak, the photon shot noise, SN_{ph}, and the read noise, N_{read}, dominate the noise level and, thus, dominate the calculation of polarimetric accuracy. However, with increase in luminous exposure, PRNU noise begins to dominate the noise level and mainly affects the polarimetric accuracy.

To reduce the random noise in the simulation, 100 images are averaged and the standard deviations of DoLP and AoLP are calculated.

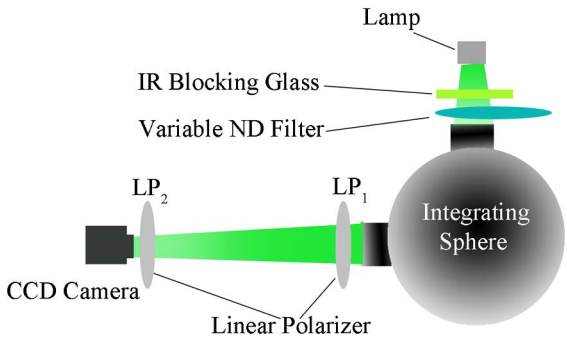

Fig. 8. Experimental setup.

We analyze the polarimetric accuracies for partially polarized light and fully polarized light with different SNRs. In the simulation, the AoLP of the incident light is arbitrarily set to 65° and the DoLP changes in the range from 0.1 to 1. Simulations of the measurement error and the standard deviation are shown in Fig. 5. It can be seen that both the relative errors and the standard deviations of the DoLP and the AoLP decrease with increase in SNR. The standard deviation of the acquired AoLP also decreases with increase in the input DoLP. However, the standard deviation of the acquired DoLP is not dependent

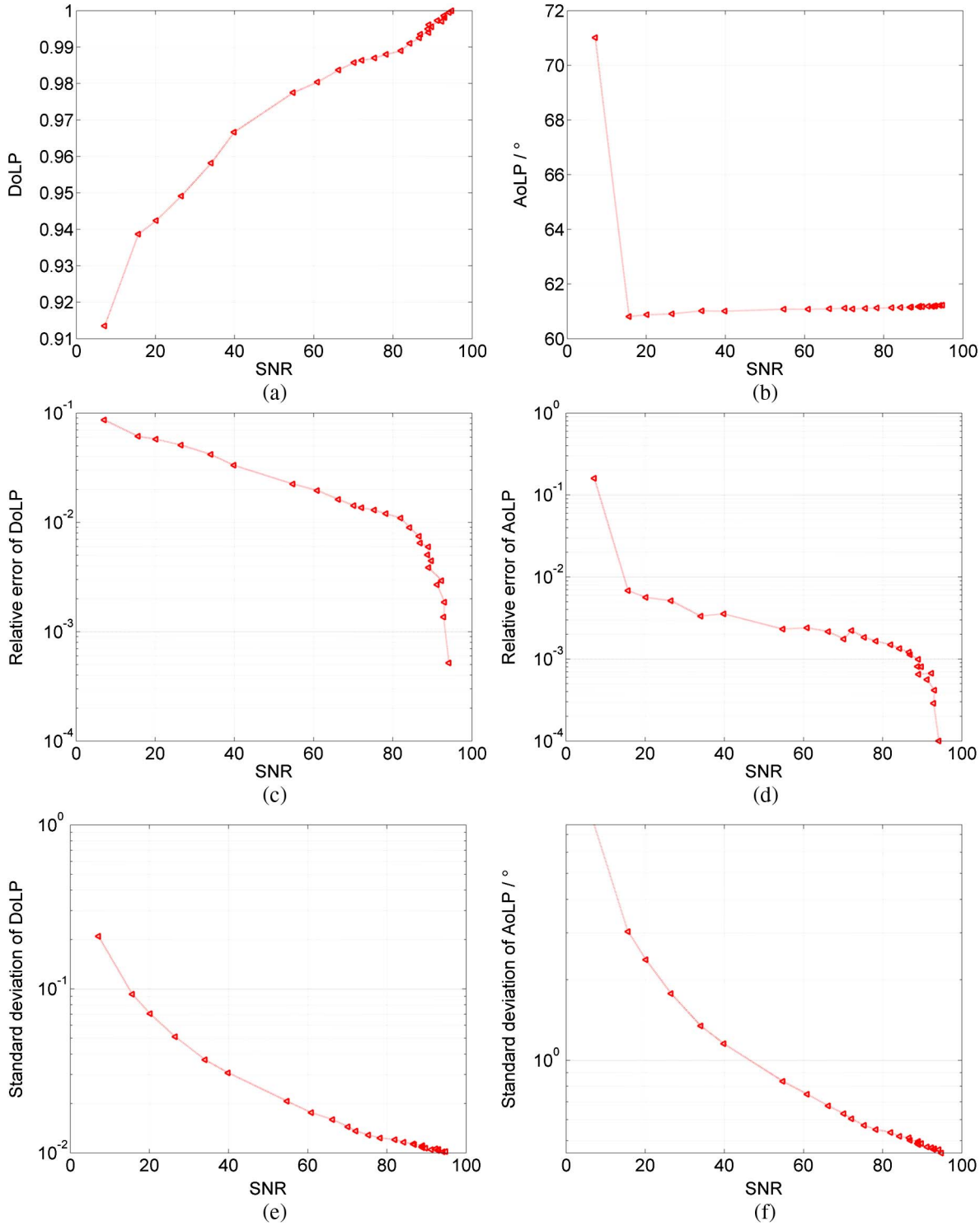

Fig. 9. Experimental results. (a) Measured DoLP versus SNR. (b) Measured AoLP versus SNR. (c) Relative error of the measured DoLP. (d) Relative error of the measured AoLP. (e) Standard deviation of the measured DoLP versus the SNR. (f) Standard deviation of the measured AoLP versus the SNR.

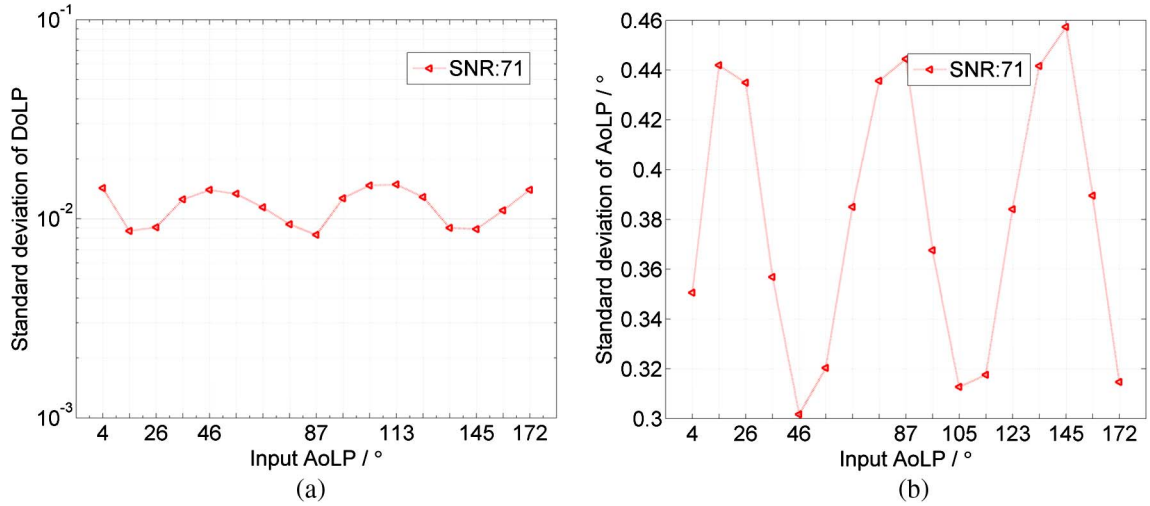

Fig. 10. Experimental results. (a) Standard deviation of the measured DoLP versus the input AoLP and (b) standard deviation of the measured AoLP versus the input AoLP.

on the input DoLP. On the other hand, even if the input DoLP is low, relatively high measurement accuracy can still be achieved with a high camera SNR. For instance, with an input DoLP of 0.1 and a SNR of 75, the measurement relative error of the DoLP is approximately 0.01 and the relative error of the AoLP is 3×10^{-4}. In Figs. 5(c) and 5(d), it can be seen that the standard deviation of the measured DoLP is mainly dependent on the camera SNR, rather than the input DoLP; the standard deviation of the measured AoLP is dependent on both the camera SNR and the input DoLP. We also investigate the effect of the input DoLP and AoLP on the measurement accuracies of the acquired DoLP and AoLP with different camera SNRs. SNR values of 133, 92, 46, 16, and 4 are chosen, which correspond to luminous exposures of 10^{-1}, 10^{-2}, 10^{-3}, 10^{-4}, and 10^{-5} lx · s, respectively, as shown in Fig. 4(b). The AoLP of the incident light is arbitrarily set to 40°. The simulation results are shown in Figs. 6 and 7. Figure 6 shows the acquired DoLP versus different input DoLPs and SNRs. Since the relative error and standard deviation of the acquired DoLP can be derived from Fig. 5, they are omitted here. Figure 7(a) shows the acquired AoLP versus different AoLPs and SNRs. The DoLP of the incident light is set to 1. Note in Fig. 7(a) the outliers around 0° and 180° when the SNR is 4. This is caused by a standard deviation of approximately 80° in the acquired AoLP near these angles, as shown in Fig. 7(c). This large standard deviation results in an incorrect calculation for the mean AoLP value. Figure 7(b) shows that with different input AoLPs, the relative error of the AoLP changes periodically at integer multiples of 30°, which is the midpoint of two analyzer orientations. The reason is that when the orientation of the linearly polarized light is at the midpoint of two analyzer orientations, two of the three images have similar intensity distributions. Figure 7(c) shows the standard deviation of the acquired AoLP. It also changes periodically, with a period of 60°, which is the angle between two analyzer orientations. One of the three images is totally dark when the orientation of the linearly polarized light is at the midpoint of two analyzer positions. Camera noise dominates the image quality; therefore, the standard deviation is maximized. On the other hand, the standard deviation of the acquired DoLP in Fig. 7(d) approaches maximum at the midpoint of two analyzer positions.

5. Experimental Demonstration

Experiments on polarization measurement were carried out to verify the simulation results. The experimental setup is shown in Fig. 8. A xenon arc lamp, IR-blocking glass, and neutral-density filters are used for the illumination path. A 6 in. integrating sphere is employed to provide uniform illumination. Two ROLYN linear polarizers (LPs) with an extinction ratio of 10,000:1 are employed. LP1 is placed in front of the integrating sphere as the polarizer to generate linear-polarization light and LP2 is placed in front of the IMPERX CCD camera as the polarization-state analyzer. For each value of output intensity, three images are captured to calculate the polarization state as described in Section 3. Since the setup can only generate fully linearly polarized light with various intensities and polarization angles, the input DoLP is 1. In the experiment, the orientation of LP1 is set arbitrarily. The experimental results are shown in Fig. 9. It can be seen that the relative errors of measured DoLP and AoLP have similar trends to the simulation results in Fig. 5. The standard deviations of the measured DoLP and AoLP match well with the simulation results. However, the acquired DoLP and AoLP have larger measurement errors, especially at high SNRs. Possible causes for these large errors include (1) the noise level of the IMPERX camera, which may be higher than the level used in the simulation, and

(2) an unstable light source. Figure 10 shows the experimental results of the standard deviations of the measured DoLP and AoLP versus the AoLP. Comparing with Figs. 7(c) and 7(d), it can be seen that the measured data have the same deviation distribution and match well with the simulation results.

6. Conclusion

We have developed a polarization noise calculation method based on a CCD camera noise model and the polarization imaging theory. The impact of the CCD camera noise on the DoLP and AoLP measurement accuracy has been simulated and analyzed. The simulation results show that with the same SNR, higher measurement accuracy can be achieved with a higher input DoLP. On the other hand, the measurement errors and standard deviations caused by the CCD camera noise decrease with increase in the SNR. For an input DoLP smaller than 0.1, the SNR should be at least 75 in order to acquire a relative error of less than 0.01. While for an input DoLP of larger than 0.5, a SNR of 15 is adequate to acquire the same accuracy. The standard deviations of both the acquired DoLP and AoLP are mainly dependent on the camera SNR.

The study provides a useful tool for polarimetry system design and optimization, as well as for polarization element selection in precise polarization measurement applications.

This work is supported by a grant from the China Scholarship Council.

References

1. J. S. Tyo, M. P. Rowe, E. N. Pugh, and N. Engheta, "Target detection in optically scattering media by polarization-difference imaging," Appl. Opt. **35**, 1855–1870 (1996).
2. S. Tominaga and A. Kimachi, "Polarization imaging for material classification," Opt. Eng. **47**, 123201 (2008).
3. J. S. Tyo, D. L. Goldstein, D. B. Chenault, and J. A. Shaw, "Review of passive imaging polarimetry for remote sensing applications," Appl. Opt. **45**, 5453–5469 (2006).
4. K. M. Twietmeyer, R. A. Chipman, A. E. Elsner, Y. Zhao, and D. VanNasdale, "Mueller matrix retinal imager with optimized polarization conditions," Opt. Express **16**, 21339–21354 (2008).
5. M. W. Kudenov, M. J. Escuti, N. Hagen, E. L. Dereniak, and K. Oka, "Snapshot imaging Mueller matrix polarimeter using polarization gratings," Opt. Lett. **37**, 1367–1369 (2012).
6. J. S. Tyo, "Design of optimal polarimeters: Maximization of signal-to-noise ratio and minimization of systematic error," Appl. Opt. **41**, 619–630 (2002).
7. D. A. Haner, B. T. McGuckin, and C. J. Bruegge, "Polarization characteristics of Spectralon illuminated by coherent light," Appl. Opt. **38**, 6350–6356 (1999).
8. N. Riviere, R. Ceolato, and L. Hespel, "Multispectral polarized BRDF: Design of a highly resolved reflectometer and development of a data inversion method," Opt. Appl. **42**, 7–22 (2012).
9. Y. Yamaguchi, T. Moriyama, M. Ishido, and H. Yamada, "Four-component scattering model for polarimetric SAR image decomposition," IEEE Trans. Geosci. Remote Sens. **43**, 1699–1706 (2005).
10. Y. Zhao, P. Gong, and Q. Pan, "Object detection by spectropolarimeteric imagery fusion," IEEE Trans. Geosci. Remote Sens. **46**, 3337–3345 (2008).
11. R. A. Chipman, "Geometrical and physical optics, polarized light, components and instruments," in *Handbook of Optics*, M. Bass, ed. (McGraw-Hill, 2009).
12. M. Smith, "Polarization metrology moves beyond home-brewed solutions," Laser Focus World **40**, 123–129 (2004).
13. J. Masiero, K. Hodapp, D. Harrington, and H. Lin, "Commissioning of the dual-beam imaging polarimeter for the University of Hawaii 88 inch Telescope," Publ. Astron. Soc. Pac. **119**, 1126–1132 (2007).
14. W. Feng, Y. Ji, and L. Chen, "The impact of signal–noise ratio on degree of linear polarization measurement," Optik **124**, 192–194 (2013).
15. G. E. Healy and R. Kondepudy, "Radiometric CCD camera calibration and noise estimation," IEEE Trans. Pattern Anal. Mach. Intell. **16**, 267–276 (1994).
16. R. A. Boie and I. J. Cox, "An analysis of camera noise," IEEE Trans. Pattern Anal. Mach. Intell. **14**, 671–674 (1992).
17. J. E. Farrell, F. Xiao, P. B. Catrysse, and B. A. Wandell, "A simulation tool for evaluating digital camera image quality, image quality and performance," Proc. SPIE **5294**, 124–131 (2004).
18. K. Irie and A. E. McKinnon, "A model for measurement of noise in CCD digital-video cameras," Meas. Sci. Technol. **19**, 045207 (2008).
19. K. Irie, A. E. McKinnon, K. Unsworth, and I. M. Woodhead, "A technique for evaluation of CCD video-camera noise," IEEE Trans. Circuits Syst. Video Technol. **18**, 280–284 (2008).
20. J. E. Farrell, P. B. Catrysse, and B. A. Wandell, "Digital camera simulation," Appl. Opt. **51**, A80–A90 (2012).
21. C. F. LaCasse, J. S. Tyo, and R. A. Chipman, "Role of the null space of the DRM in the performance of modulated polarimeters," Opt. Lett. **37**, 1097–1099 (2012).
22. J. S. Tyo, "Optimum linear combination strategy for an N-channel polarization-sensitive vision or imaging system," J. Opt. Soc. Am. A **15**, 359–366 (1998).
23. http://en.wikipedia.org/wiki/Condition_number.
24. J. Mazzetta, D. Caudle, and B. Wageneck, "Digital camera imaging evaluation," Technical Report (Electro Optical Industries, 2005), available at http://www.electro-optical.com/pdf/EOI%20OSG%202005%20Paper%20final.pdf.